Turbulent forced convective cooling of microelectronic devices

A. Wietrzak and D. Poulikakos
Mechanical Engineering Department, University of Illinois at Chicago, Chicago, IL, USA

This article presents a numerical study on turbulent forced convective cooling of microelectronic devices. A two-equation k–ε model is used for the turbulent flow. The results document the effects of various design parameters on flow and heat transfer characteristics of a miniature chip or sensor such as the microbridge sensor. Flow recirculations were predicted before and after block modeling the sensor. More importantly, flow recirculation created by separation and reattachment occurs on the top face of the block, where the heating and temperature sensing elements are installed. This recirculation has a severe effect on the local heat flux at the sensor surface. The effects of block height and location (distance from the channel entrance), Reynolds number, materials comprising the block, and heater size are thoroughly investigated.

Keywords: cooling of electronic equipment; turbulent convection

Introduction

Cooling of electronic components has been a major concern of manufacturers of devices ranging from computers to all types of miniature sensors and switches. In all cases, efficient and effective cooling of electronic components is directly related to the lifetime and reliability of the device.

Accurate measurement of the flow of air or other gases is important in numerous control systems. In the late 1970s several research groups began to work on miniature silicon-based sensors to replace large conventional units. By etching tiny structures in silicon, the Honeywell team was able to design a reliable sensor on a chip. Even though this sensor is utilized to measure high velocities (on the order of 100 m/s), it is sensitive enough to measure flow velocities as low as a few inches per minute.

The heart of the sensor is a double microbridge made of silicon nitride, which carries the heater and the detectors. The microbridge is only 1 mm or 2 mm long, or too small for the details of its structure to be seen by the unaided eye. The most novel feature of the sensor is the pit etched in the silicon under the microbridge. The pit provides efficient thermal insulation for the heater. Only a small power input is needed to raise the temperature of the microbridge considerably above the chip temperature. Figure 1(a) shows a diagrammatic representation of a sensor as it is placed in a housing, ready to be used for flow measurements. A cross section of the left-hand end of the sensor-housing assembly (section A–A in Figure 1a) is shown in Figure 1(b). In terms of heat transfer and fluid mechanics, the flow around the sensor chip can be modeled as flow around a rectangular object placed at the bottom wall of a parallel-plate channel.

The complexity and practical importance of predicting the flow pattern of a fluid flowing over an obstruction, whether in an open or closed channel, have caused this topic to be the subject of several theoretical and experimental investigations. Perhaps one of the earliest numerical papers on the subject was that of Harlow and Welch.[1] They investigated a time-dependent, laminar, incompressible, free surface flow over a square obstacle. Included in their work was a novel procedure of displacing the velocity nodes with respect to the pressure nodes, which later became known as the "staggered grid" formulation.[2] More recently, Davalath and Bayazitoglu[3] studied numerically the conjugate heat transfer for two-dimensional (2-D) developing flow over a sequence of three rectangular heat generating blocks placed in a parallel-plate channel. Their work was confined to laminar incompressible flow. A similar study was conducted by Zebib and Wo.[4]

Many investigations of turbulent recirculating flows have been concerned principally with testing turbulence models, particularly the k–ε model. Durst and Rastogi[5] and Gosman *et al.*[6] tested the k–ε model for flows over a square block, and for channels with rib-roughened surfaces, respectively. After comparing with experimental measurements, Durst and Rastogi[5] concluded that the present state of turbulence modeling of flows with separation is rather good, although some flows still cannot be predicted accurately. Gosman *et al.*[6] determined that the two-equation turbulence model provides adequate precision for

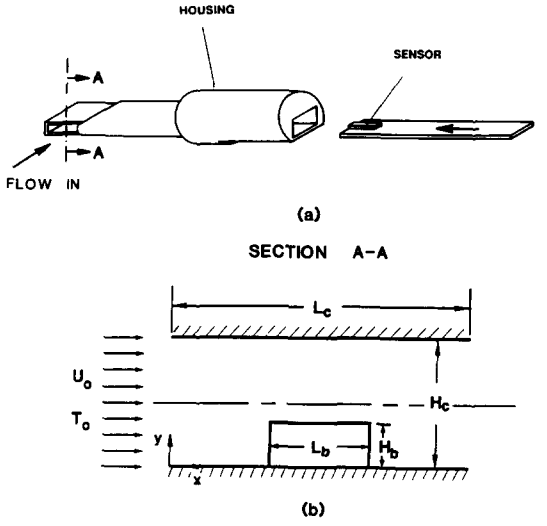

Figure 1 (a) Diagrammatic representation of a sensor as it is inserted into a housing. The entire assembly is placed in a fluid-carrying channel. (b) Section A–A of the left end of the sensor-housing assembly in (a): A diagrammatic illustration

Address reprint requests to Dr. Poulikakos at the Mechanical Engineering Department, University of Illinois at Chicago, P.O. Box 4348, Chicago, IL 60680, USA.

Received 31 August 1989; accepted 8 January 1990

many engineering applications; however, it was found to be deficient in predicting detailed flow patterns. Other investigators have concentrated on testing the k–ε model for forward and backward facing steps. Castro[7] concluded that inadequate turbulence models are not the sole, or even perhaps the major, cause of discrepancies between prediction and experiment. Locally, the most significant role is played by truncation errors arising from finite-differencing the governing equations. The errors cannot easily be reduced to insignificance, particularly near sharp corners, owing to the grid size often used in the investigations. Chieng and Launder[8] and Gooray *et al.*[9] were concerned primarily with using a low Reynolds number version of the k–ε model to predict the recirculating flow pattern downstream of a backward facing step. Overall, the model was found to be a viable alternative to the more complex schemes involving higher order turbulent closures.

Most of these investigators were concerned principally with studying the accuracy with which the k–ε model can predict turbulent flows. Because of its successful performance, as well as its relative simplicity and adaptability, this model is, arguably, the most popular model used in numerical prediction of turbulence flow and heat transfer today. In this study, the k–ε model is used to predict the effects of turbulent flow on the heat transfer characteristics of a miniature rectangular chip.

Mathematical formulation

The configuration of the problem under investigation is depicted in Figure 1(b). Because of the abrupt changes in geometry, regions of recirculation and separation are expected to occur in the flow field in the immediate vicinity of the block. Consequently, the boundary layer versions of the governing conservation equations cannot be used because of their parabolic nature. Thus retaining all the terms in the governing equations and keeping them in the elliptic form is necessary. The range of the Reynolds numbers used in this investigation lies between 700 and 12×10^3, from the laminar to well into the turbulent flow regime.[10] For the results presented here, the governing equations take into account the assumption that the flow is turbulent. The additional assumptions made are that the plates and block are smooth, the flow is 2-D, and the fluid is incompressible with constant physical properties.

The form of the k–ε model proposed by Jones and Launder[11,12] is used in this study because of its demonstrated success in forced convection problems. This model is presented in dimensionless form. Subsequently, necessary details explaining some of the terms are presented. All variables are defined in the Notation box. The nondimensionalization was based on the following definitions:

$$x^*=\frac{x}{H_c},\ y^*=\frac{y}{H_c},\ L_c^*=\frac{L_c}{H_c},\ H_b^*=\frac{H_b}{H_c},\ u^*=\frac{u}{U_o},\ v^*=\frac{v}{U_o}$$

$$p^*=\frac{p}{\rho U_0^2},\qquad \nu_t^*=\frac{\nu_t}{\nu},\ \nu_{\text{eff}}^*=\frac{\nu_{\text{eff}}}{\nu} \tag{1}$$

$$k^*=\frac{k}{U_0^2},\qquad \varepsilon^*=\frac{\varepsilon H_c^2}{U_0^2\nu},\qquad \theta=\frac{T-T_o}{T_o},\qquad k_s^*=\frac{k_s}{k_f}$$

The asterisks denoting dimensionless quantities are dropped at this point for convenience. All quantities in the following equations are dimensionless. The following are the dimensionless governing conservation equations.

- *Continuity equation:*

$$\frac{\partial u}{\partial x}+\frac{\partial v}{\partial y}=0 \tag{2}$$

- *Momentum equation in the x-direction:*

$$\frac{\partial(uu)}{\partial x}+\frac{\partial(uv)}{\partial y}=-\frac{\partial p}{\partial y}+\frac{\partial}{\partial x}\left(\frac{\nu_{\text{eff}}}{\text{Re}}\frac{\partial u}{\partial x}\right)+\frac{\partial}{\partial y}\left(\frac{\nu_{\text{eff}}}{\text{Re}}\frac{\partial u}{\partial y}\right)$$
$$+\frac{1}{\text{Re}}\left(\frac{\partial u}{\partial x}\frac{\partial \nu_t}{\partial x}+\frac{\partial v}{\partial x}\frac{\partial \nu_t}{\partial y}\right)-\frac{2}{3}\frac{\partial k}{\partial x} \tag{3}$$

Notation

c_p	Fluid specific heat at constant pressure
E_φ	Error in convergence criterion for variable φ
H	Height
k	Turbulence kinetic energy
k_f	Thermal conductivity of the fluid
k_s	Thermal conductivity of the solid block
L	Length
Nu	Local Nusselt number, Equation 28
P	Mean pressure
$\dot{q}$	Heat generation rate
Re	Reynolds number, Equation 9
R_t	Turbulent Reynolds number
S	Dimensionless source term, $\dot{q}H^2{}_c/(T_o k_f)$
T	Mean temperature
u	Mean horizontal velocity component
U_o	Inlet velocity
v	Mean vertical velocity component
x	Horizontal coordinate
x'	Distance around periphery of the block, starting from the bottom corner of the upstream face
y	Vertical coordinate

Greek symbols

α	Thermal diffusivity, $k_f/\rho c_p$
ε	Turbulence kinetic energy dissipation rate
θ	Mean dimensionless temperature
μ	Dynamic viscosity
ν	Kinematic viscosity
ρ	Density
σ	Prandtl number, $\frac{\nu}{\alpha}$
σ_t	Turbulent Prandtl number
φ	General variable
ω	Relaxation parameter

Subscripts

b	Block
c	Channel
f	Fluid
o	Inlet
t	Turbulent
w	Wall
*	Dimensionless quantity

Symbols

′	Dimensionless length around periphery of the block

- *Momentum equation in the y-direction:*

$$\frac{\partial(uv)}{\partial x}+\frac{\partial(uv)}{\partial y}=-\frac{\partial p}{\partial y}+\frac{\partial}{\partial x}\left(\frac{\nu_{\text{eff}}}{\text{Re}}\frac{\partial v}{\partial x}\right)+\frac{\partial}{\partial y}\left(\frac{\nu_{\text{eff}}}{\text{Re}}\frac{\partial v}{\partial y}\right)+\frac{1}{\text{Re}}\left(\frac{\partial v}{\partial y}\frac{\partial \nu_t}{\partial y}+\frac{\partial u}{\partial y}\frac{\partial \nu_t}{\partial x}\right)-\frac{2}{3}\frac{\partial k}{\partial y} \quad (4)$$

- *Turbulence kinetic energy (k) equation:*

$$\frac{\partial(uk)}{\partial x}+\frac{\partial(vk)}{\partial y}=\frac{\partial}{\partial x}\left(\frac{1+\nu_t/\sigma_k}{\text{Re}}\frac{\partial k}{\partial x}\right)+\frac{\partial}{\partial y}\left(\frac{1+\nu_t/\sigma_k}{\text{Re}}\frac{\partial k}{\partial y}\right)+\frac{1}{\text{Re}}\left[\nu_t G-\varepsilon-2\left\{\left(\frac{\partial k^{1/2}}{\partial x}\right)^2+\left(\frac{\partial k^{1/2}}{\partial y}\right)^2\right\}\right] \quad (5)$$

- *Turbulence dissipation rate (ε) equation:*

$$\frac{\partial(u\varepsilon)}{\partial x}+\frac{\partial(v\varepsilon)}{\partial y}=\frac{\partial}{\partial x}\left(\frac{1+\nu_t/\sigma_k}{\text{Re}}\frac{\partial \varepsilon}{\partial x}\right)+\frac{\partial}{\partial y}\left(\frac{1+\nu_t/\sigma_k}{\text{Re}}\frac{\partial \varepsilon}{\partial y}\right)+\frac{1}{\text{Re}}\left\{C_{\varepsilon_1}\nu_t\frac{\varepsilon}{k}G-C_{\varepsilon_2}f_2\frac{\varepsilon^2}{k}+2\nu_t\left[\left(\frac{\partial^2 u}{\partial x^2}\right)^2+\left(\frac{\partial^2 u}{\partial y^2}\right)^2+\left(\frac{\partial^2 v}{\partial x^2}\right)^2+\left(\frac{\partial^2 v}{\partial y^2}\right)^2\right]\right\} \quad (6)$$

- *Energy equation for the fluid:*

$$\frac{\partial(u\theta)}{\partial x}+\frac{\partial(v\theta)}{\partial y}=\frac{\partial}{\partial x}\left\{\left[\left(\frac{\nu_t}{\sigma_t}+\frac{1}{\sigma}\right)/\text{Re}\right]\frac{\partial\theta}{\partial x}\right\}+\frac{\partial}{\partial y}\left\{\left[\left(\frac{\nu_t}{\sigma_t}+\frac{1}{\sigma}\right)/\text{Re}\right]\frac{\partial\theta}{\partial y}\right\} \quad (7)$$

- *Energy equation for the block:*

$$\frac{\partial}{\partial x}\left(k_s\frac{\partial\theta}{\partial x}\right)+\frac{\partial}{\partial y}\left(k_s\frac{\partial\theta}{\partial y}\right)+S=0 \quad (8)$$

In Equations 2–8,

$$\text{Re}=\frac{U_o H_c}{\nu} \quad (9)$$

$$\text{R}_t=\frac{k^2}{\varepsilon}\text{Re}^2 \quad (10)$$

$$f_1=\exp[-3.4/(1+0.02\text{R}_t)] \quad (11)$$

$$f_2=1.0-0.222\exp(-\text{R}_t^2/36) \quad (12)$$

$$\nu_t=C_\mu f_1\frac{k^2}{\varepsilon}\text{Re}^2 \quad (13)$$

$$\nu_{\text{eff}}=1+\nu_t \quad (14)$$

$$G=2\left[\left(\frac{\partial u}{\partial x}\right)^2+\left(\frac{\partial v}{\partial y}\right)^2\right]+\left(\frac{\partial u}{\partial y}+\frac{\partial v}{\partial x}\right)^2 \quad (15)$$

Several empirical constants (C_μ, C_{ε_1}, C_{ε_2}, σ_k, and σ_ε) appear in Equations 9–15. The values of these constants as recommended by Jones and Laudner[11] are given in Table 1. In Table 1, also, the values of the Prandtl number (σ) and the turbulence Prandtl number (σ_t) are reported. The values of these parameters are especially appropriate for channel flows like the one encountered in the present study.[11] Equations 2–15 are general and is valid in the near wall region. This is a desirable feature because no laws of wall are needed.[11]

The following are the boundary conditions necessary to complete the formulation of the problem.

- *For the velocity field:*

$$x=0;\ 0<y<1:\ u=1;\ v=0 \quad (16)$$

Table 1 Values of constants in the k–ε turbulence model

Constant in turbulence model	Value
C_μ	0.09
C_{ε_1}	1.44
C_{ε_2}	1.92
σ	0.7
σ_k	1.0
σ_t	0.9
σ_ε	1.3

$$x=\frac{L_c}{H_c};\ 0<y<1:\ \frac{\partial u}{\partial x}=0;\ \frac{\partial v}{\partial x}=0 \quad (17)$$

$$0<x<\frac{L_c}{H_c},\ \text{on all solid boundaries:}\ u=v=0 \quad (18)$$

- *For the turbulence kinetic energy and dissipation equations:*

$$x=0;\ 0<y<1:\ k=0.0275;\ \varepsilon=\frac{k^{3/2}}{0.005}\text{Re} \quad (19)$$

$$x=\frac{L_c}{H_c};\ 0<y<1:\ \frac{\partial k}{\partial x}=0;\ \frac{\partial \varepsilon}{\partial x}=0 \quad (20)$$

$$0<x<\frac{L_c}{H_c};\ \text{on all solid boundaries:}\ k=\varepsilon=0 \quad (21)$$

- *For the energy equation (fluid and block):*

$$x=0;\ 0<y<1:\ \theta=0 \quad (22)$$

$$x=\frac{L_c}{H_c};\ 0<y<1:\ \frac{\partial\theta}{\partial x}=0 \quad (23)$$

$$0<x<\frac{L_c}{H_c};\ y=0:\ \frac{\partial\theta}{\partial y}=0 \quad (24)$$

$$0<x<\frac{L_c}{H_c};\ y=1:\ \frac{\partial\theta}{\partial y}=0 \quad (25)$$

$$\text{At the fluid–block interface:}\ \frac{k_s}{k_f}\left(\frac{\partial\theta}{\partial n}\right)_s=\left(\frac{\partial\theta}{\partial n}\right)_f;\ \theta_s=\theta_f \quad (26)$$

We neglected natural convection effects in this study—and justifiably so—because the typical Reynolds number for most of the numerical calculations is Re = 6000, which corresponds to velocities on the order of 100 m/s.

Numerical solution

The governing equations and boundary conditions were made discrete by a control-volume finite-difference method. The numerical solution was obtained by using the general principles of the SIMPLER algorithm outlined in great detail in Patankar.[2,13]

The thermal conductivity of the block simulating the sensor is not constant (it depends on the composition of the sensor), so a harmonic mean approximation[2,13] was used to obtain the interface conductivity between two control volumes of different conductivity in making Equation 8 discrete. The convective and diffusive fluxes were approximated using the power law scheme,[2] whereby, upon integrating the governing equations over a control volume, the exact solution of the Burgers equation is used to calculate the fluxes at the control volume surfaces. This approach allows a more judicious approximation

of the fluxes than either a hybrid or upwind scheme would provide.

The discrete conservation equations are solved by using two different iteration methods. Specifically, the momentum, k, and ε equations are solved using a tridiagonal matrix algorithm (TDMA). The TDMA is applied to the grid lines in the y direction. The energy and the pressure correction equations are solved using the Gauss–Seidel point-by-point iterative scheme. For both methods, the direction of iteration is alternated so that the solution proceeds from left to right and vice versa. For the Gauss–Seidel scheme, the y-direction of iteration is also alternated. Use of the two different schemes was necessary to obtain a faster convergence rate.

Because of the large variations in the source terms, underrelaxation was necessary for the dependent variables and the source terms to achieve convergence (Doormaal and Raithby[14]). A typical value of the underrelaxation parameters was $\omega = 0.4$. This value is within the range recommended by Patankar.[2]

The solution was assumed to be converged when the following criterion was satisfied:

$$\frac{\sum_{j=1}^{m}\sum_{i=1}^{n}|\varphi_{i,j}^{k+1}-\varphi_{i,j}^{k}|}{\sum_{j=1}^{m}\sum_{i=1}^{n}|\varphi_{i,j}^{k}|} \leq E_{\varphi} \tag{27}$$

where E_{φ} is a prescribed error. The value $E_{\varphi}=5\times10^{-4}$ was used for the majority of the runs. Selection of the value of E_{φ} takes into account the fact that the rather strong underrelaxation leads to small changes from iteration step to iteration step. In addition, the converged velocity field had to satisfy continuity within prescribed error, both locally (at each control volume) and globally (the mass flow rate calculated at any cross section of the channel, such as the inlet and the outlet, had to be constant).

A nonuniform grid was used in both the vertical and the horizontal directions. A typical grid spacing consisted of 65 vertical and 35 horizontal grid lines. The neighborhood of the block is populated densely with grid lines. Grid spacing resulted from a trial-and-error procedure. Numerous details on grid fineness are included in ref. 13 but not repeated here because of space limitations. Our grid spacing is finer than that of Durst and Rastogi[5] (they used 50×27 for a similar problem of turbulent flow over a block), who proved their grid to be adequate by reproducing experimental results with acceptable accuracy. Furthermore, results of runs made with finer grids (80×44) showed no significant improvement.[13] Overall, grid fineness was a compromise between accuracy and computational time (typical runs required about 6000 s CPU time on an IBM 3081).

The numerical code was tested against previous studies for laminar flow over three heat generating blocks in a channel (Davalath and Bayazitoglu[3]), and the agreement was found to be very good. In addition, the code was tested successfully against the experimental results of Emery and Gessner[15] for turbulent flow between two parallel plates. Details on these and other tests of the numerical code are included in Wietrzak.[13]

The heat transfer results of this study are presented in terms of the local Nusselt number at the block surface, defined as

$$\mathrm{Nu}=\frac{-(\partial\theta/\partial n)_w}{\theta_w} \tag{28}$$

where n is the direction normal to the block surface. The local temperature gradient in Equation 28 was evaluated using a three-point Taylor series expansion.

Results and discussion

The configuration of the miniature chip in operation (geometry, composition, location in the channel, and flow conditions) offers a large number of parameters to be investigated. It was therefore necessary to limit the scope of the study to those parameters that are expected to have a significant effect on the cooling process of the chip (microbridge sensor). The configurations of interest are summarized in Table 2. The value of the heat generation term in Equation 8 was held constant at $S=400$ throughout the study. This value is representative of typical operating conditions for sensors or other chips. In addition, the inlet value of ε, Equation 19, is generally dependent on channel diameter. As mentioned earlier, the small sensor housing (channel) is placed inside a much larger fluid-carrying channel in real applications. Hence the diameter of this larger channel was used to calculate ε at the test section inlet. A typical value of the outer diameter is 15 cm and of the sensor housing 0.5 cm, which makes the ratio of the two diameters 1:30. With this information, the relation for ε in Equation 19 was obtained from Gosman *et al.*[6]

We used configuration 1 in Table 2 as the base run for the flow field for $\mathrm{Re}=6000$, and the working fluid was air. In presenting the results for isotherms and streamlines, we decided to focus on the *vicinity of the chip* rather than presenting the temperature and velocity field in the whole channel (from inlet to exit). This decision enabled us to capture a reasonable amount of detail of the temperature and flow fields in the important region near the sensor. The streamline pattern in the regions well ahead and well after the sensor is typical for flows in channels and does not offer significant additional information.

The streamline map of Figure 2(a) indicates that recirculations develop before and after the sensor. The recirculation after the sensor is considerably larger, but, more importantly, a pocket of recirculating fluid develops on the top surface of the sensor.

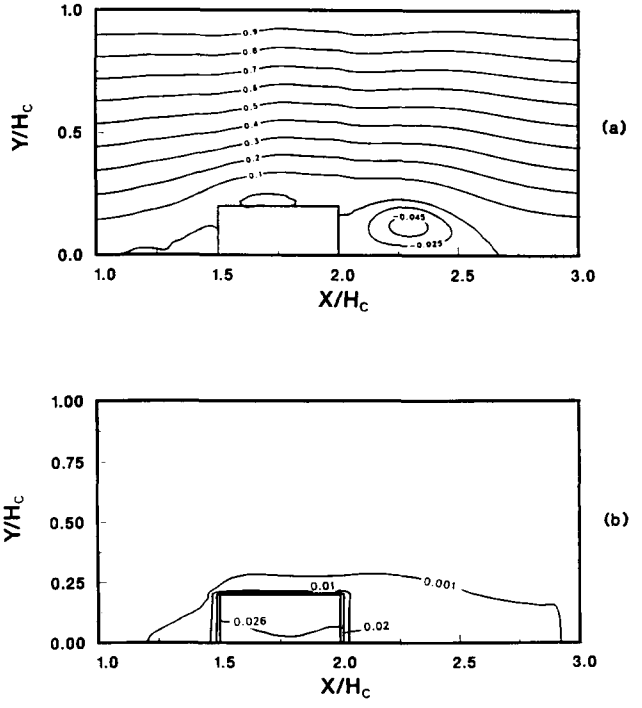

Figure 2 Configuration 1 (Table 2) with $\mathrm{Re}=6000$ and the upstream side of the block at $x/H_c=1.5$: (a) streamlines; (b) isotherms

Table 2 Summary of chip configurations

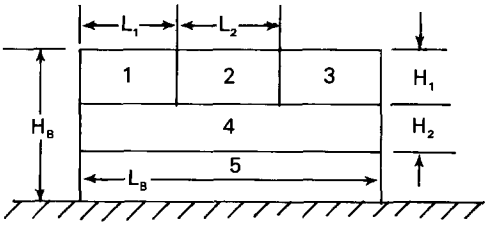

Configuration Number	$\frac{H_B}{H_c}$	$\frac{H_1}{H_c}$	$\frac{H_2}{H_c}$	$\frac{L_B}{H_c}$	$\frac{L_1}{H_c}$	$\frac{L_2}{H_c}$
1	0.2	0.02	0	0.5	0	0.5
2	0.2	0.02	0	0.5	0	0.5
3	0.2	0.02	0.02	0.5	0	0.5
4	0.2	0.02	0.04	0.5	0	0.5
5	0.2	0.02	0.02	0.5	0.10	0.3
6	0.2	0.02	0.02	0.5	0.10	0.3
7	0.3	0.02	0.02	0.5	0	0.5

	Material of the various block sections†					Heat Generating Sections
	1	2	3	4	5	
1		Silicon			Silicon	1, 2, 3
2		Plastic Compound			Plastic Compound	1, 2, 3
3	Composite	Composite	Composite	Air	Silicon	1, 2, 3
4	Composite	Composite	Composite	Air	Silicon	1, 2, 3
5	Composite	Composite	Composite	Air	Silicon	2
6	Air	Composite	Air	Air	Silicon	2
7	Composite	Composite	Composite	Air	Silicon	1, 2, 3

† *Material* — *Thermal Conductivity* (W/m·K)

Composite (silicon nitride)	11.00
Silicon	120.00
Plastic compound	0.14
Air	0.03

This type of behavior has been observed both experimentally and numerically in modeling of flows involving separation (Durst and Rastogi[5]). As the heating elements of the sensor are installed at the top surface, the recirculation pocket at the top wall of the block should have a significant effect on heat transfer.

Figure 2(b) shows a map of isotherms corresponding to the streamlines of Figure 2(a). The heating effect of the channel is present both upstream and downstream, as small temperature variations are observed throughout the sensor. The block faces are isothermal, as also shown in Figure 3(a). The reason is that in configuration 1 in Table 2 the material of the block is silicon, which is about 4000 times more conductive than air.

The local Nusselt number distribution is shown in Figure 4. The Nusselt number variation along the block is particularly significant along the top surface, where the heating takes place. The "hump" in the Nusselt number in this region is a direct result of flow recirculation along the top surface and has severe implications on the cooling of an electronic component. In the absence of recirculation, the Nusselt number would decrease monotonically along the top surface, as laminar flow studies indicate (Davalath and Bayazitoglu[3]). As expected, the maximum Nu occurs at the leading-edge corner of the top face, where the fluid turns sharply and a boundary layer starts forming. Figures 3(a) and 4 predict that, although heat is not being removed uniformly along the surface of the block, its high conductivity prevents hot spots from forming.

The Nusselt number distributions for configurations 2–5 in Table 2 are qualitatively similar to that discussed above in connection with configuration 1 (Figure 4). For the sake of brevity, we do not report Nusselt number distributions for configurations 2–5; these distributions are included in Wietrzak.[13]

Figures 3(b) and 5(a) correspond to configuration 2 in Table 2 and show the effect of using a low-conductivity material to construct the block. This time, the material of the block (commonly used in the mold of IC chips) is only five times more conductive than air. Figures 5(a) and 3(b) suggest that the block and its surface are significantly nonisothermal. The hottest region in the block is located at the top mid-section (Figure 5a).

In order to allow for a sufficient rise in the temperature of the silicon nitride bridge (top surface of the block) in the case of the microbridge sensor, a gap of air separates the heater from its silicon base. Because of the small size of the whole assembly, the air gap is assumed to remain stagnant. This arrangement was modeled by configuration 3 in Table 2. The thermal conductivity of the strip at the top surface of the block is approximately 370 times that of air. Consequently, as Figures 3(c) and 5(b) indicate, the temperature on top of the block is uniform and similar to that in configuration 1. However, the air film acts as an insulator. Thus, the temperature of the top surface is much higher than that of the rest of the block. Figures 3(c) and 5(b) show clearly the insulating effect of the air gap.

Configuration 4 in Table 2 was used to study the effect of increasing the air-gap thickness. Figures 3(d) and 5(c) show the main results. The surface temperature of the block has increased considerably over that of configuration 3. Otherwise, qualitatively, the profiles have remained the same. Hence, in order to allow for the heat generating top surface to reach a

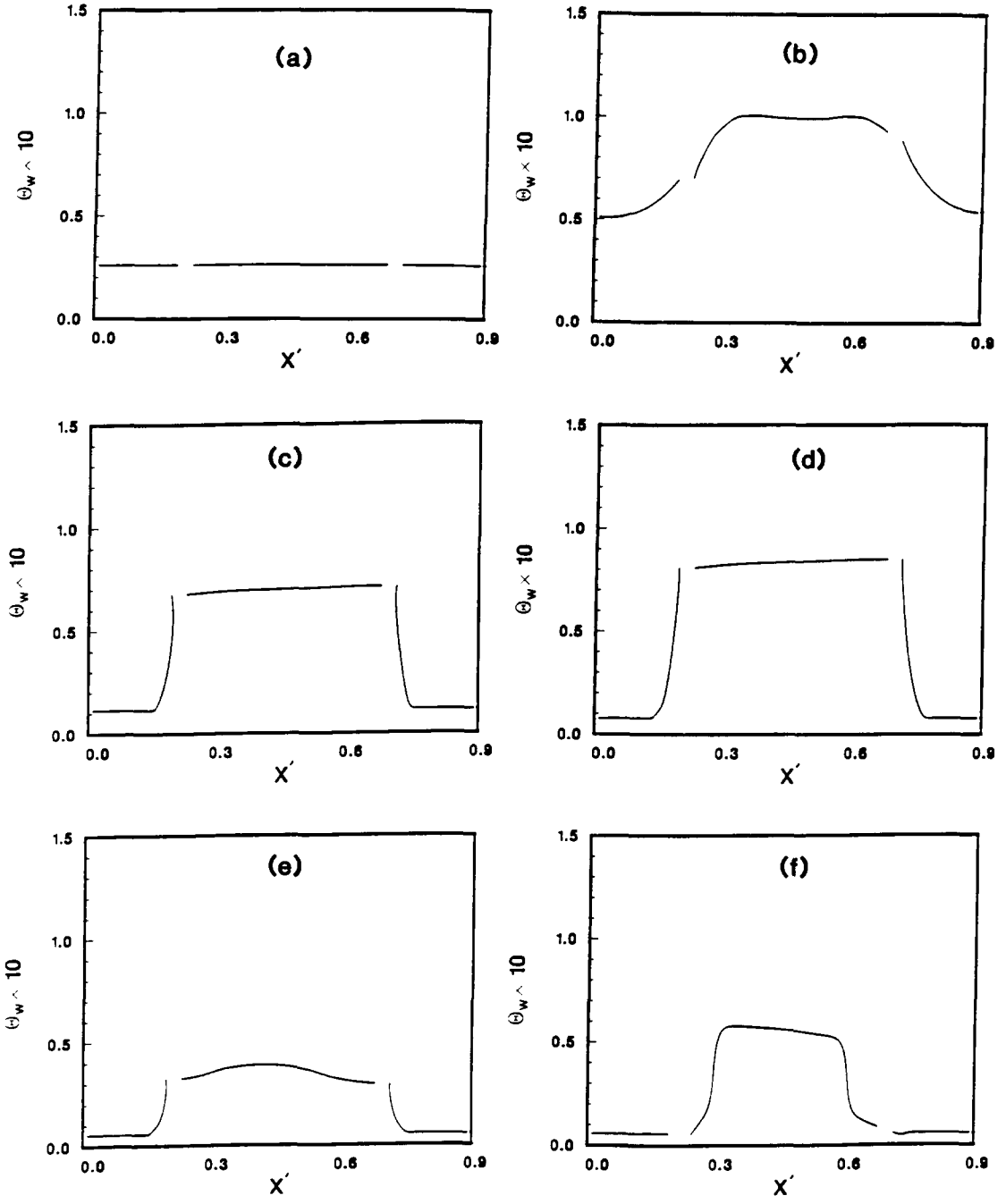

Figure 3 Surface temperature variation of the sensor when its upstream face is located at $x/H_c = 1.5$ and for Re = 6000: (a) configuration 1; (b) configuration 2; (c) configuration 3; (d) configuration 4; (e) configuration 5; (f) configuration 6. All configurations are defined in Table 2

significantly higher temperature, and at the same time isolate this thermal effect from the rest of the sensor, the air gap should be increased.

Configuration 5 in Table 2 was used to study the effect of the length of the heat generating portion of the top surface of the sensor. The isotherm plot, Figure 5(d), shows a distinct rise in the temperature just below the heating element, implying that a hot region has developed underneath the heater. According to Figure 3(e) the surface temperature peaks in the heater vicinity. However, the maximum temperature is less than that for configuration 3. The reason is that the top surface is only partially generating heat. Configuration 6 in Table 2 was used to predict the rise in temperature of the top surface when the conductivity of the material surrounding the heat generating region is decreased. As shown in Figure 3(f), the temperature increases greatly compared to that of configuration 5. In fact, the top surface temperature is comparable in magnitude to that of configuration 3. However, the temperature increases of the front and back surfaces of the sensor are smaller.

The effect of the position of the block relative to the entrance was examined next. Configuration 3 was used, and the block was located farther away (three channel diameters) from the entrance. The flow pattern, Figure 6(a), has changed in that the recirculation on top of the block is flatter, recirculation in front of the block has decreased, and the recirculating zone behind the block covers almost the entire back surface. This

change has a direct impact on Nusselt number variation, as shown in Figure 6(b). No clear "hump" exists on the Nu curve segment along the top surface. The reduction of this hump is caused by a change in the shape of the recirculation on the top face of the block from that in Figure 4(a). Clearly, this recirculation severely affects the Nusselt number. The temperature distribution inside the block and at the top surface, not shown for brevity, did not change noticeably compared to the case in which the block was located $1\frac{1}{2}$ channel diameters from the inlet (Figures 3c and 5b).

Changing the height of the block (configuration 7) had a significant impact on the recirculation zones. Figure 7(a) shows that the recirculations on top of the block and behind it have strengthened appreciably. Figures 7(b) and 8(a) display temperature results. The surface temperature has not changed significantly from that of configuration 3. The Nusselt variation, Figure 8(b), has adjusted to reflect the change in the flow field. The Nusselt number changes more gradually across the recirculation zone on top of the block, compared to earlier configurations. In addition, as the right edge is approached, the magnitude of Nu is significantly larger than that, for example, in configuration 3.

The final simulation was made to examine the effect of increasing the Reynolds number. Configuration 3 for Re = 12000 was used.[13] Because of space limitations, results of this

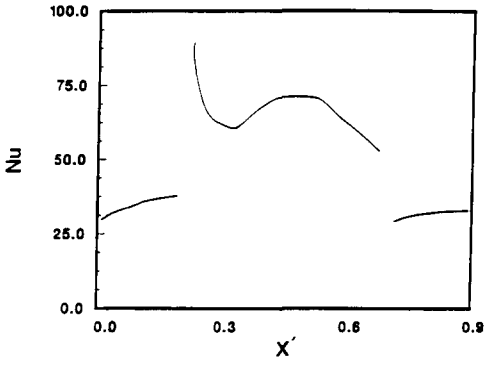

Figure 4 Local Nusselt number variation at the surface of the sensor when its upstream face is located at $x/H_c = 1.5$ and for Re = 6000 (configuration 1)

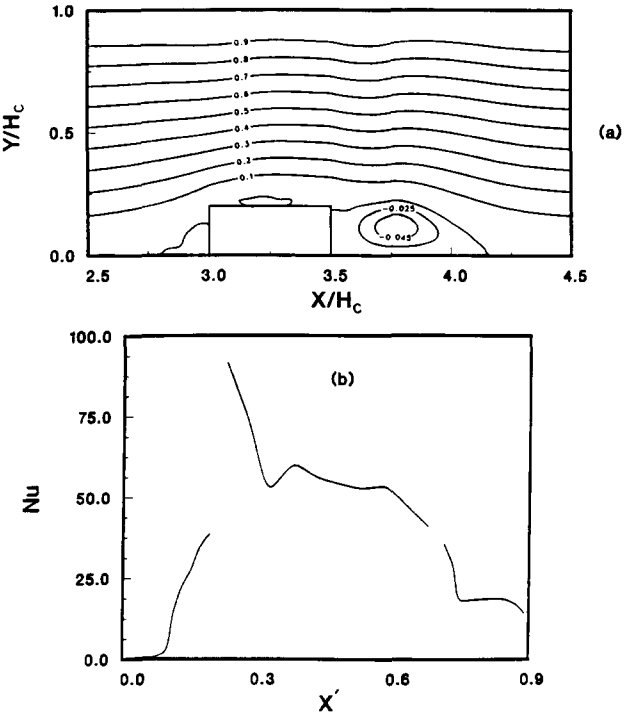

Figure 6 Configuration 3 for Re = 6000 and when the upstream surface of the sensor is located at $x/H_c = 3$: (a) streamlines; (b) local Nusselt number distribution along the surface

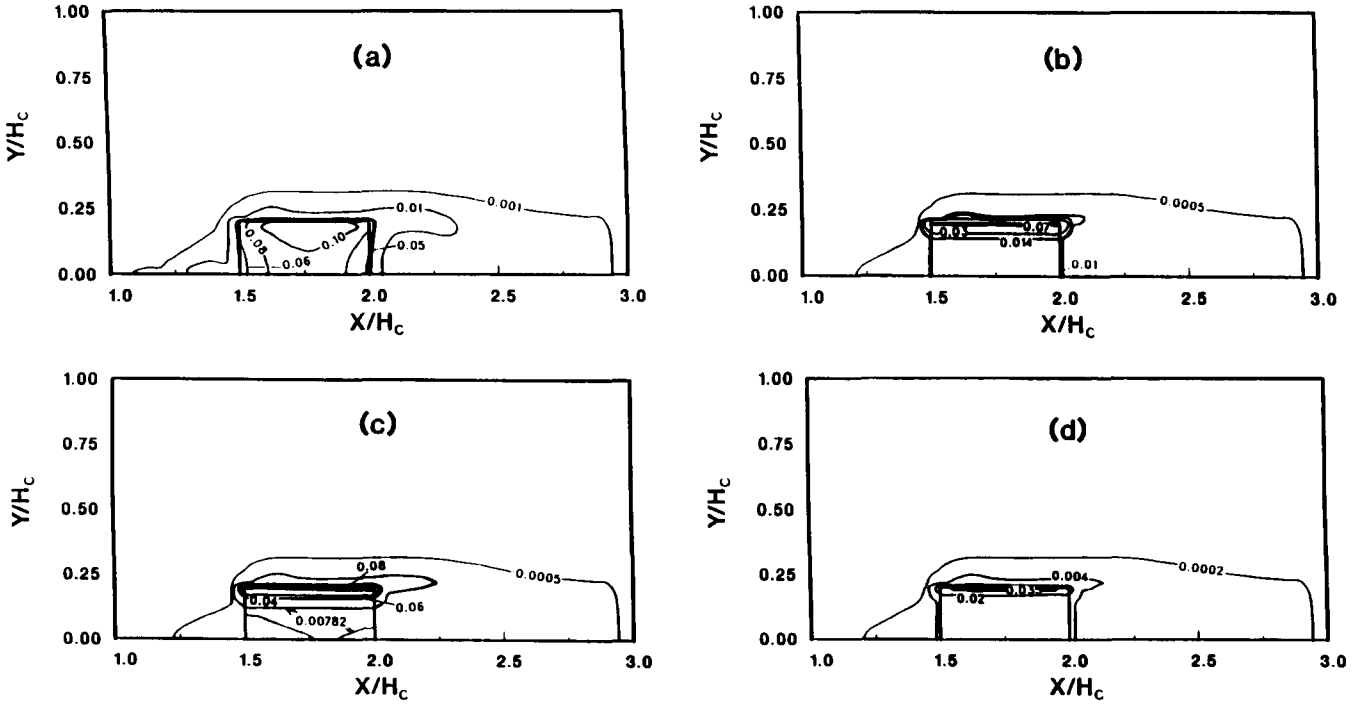

Figure 5 Isotherm maps for the sensor located at $x/H_c = 1.5$ and for Re = 6000: (a) configuration 2; (b) configuration 3; (c) configuration 4; (d) configuration 5. All configurations are defined in Table 2

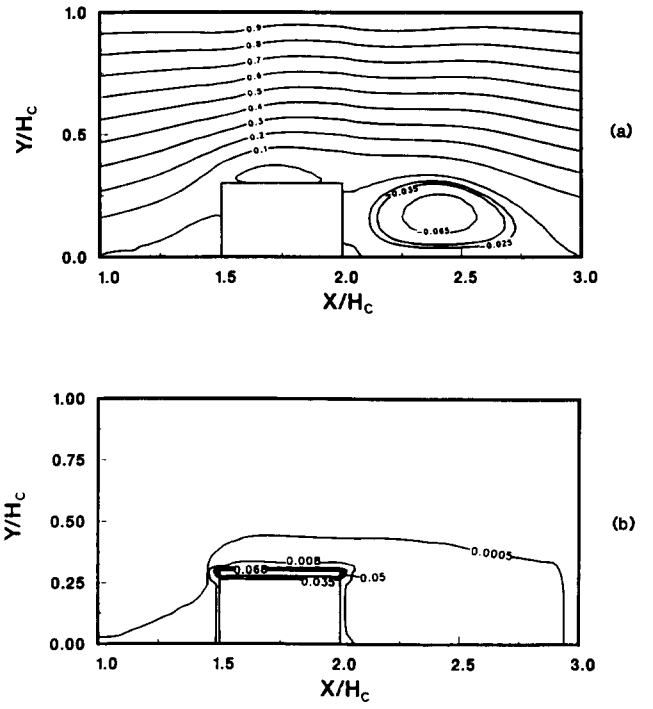

Figure 7 Configuration 7 (Table 2) with Re=6000 and the upstream face of the sensor at $x/H_c=1.5$: (a) streamlines; (b) isotherms

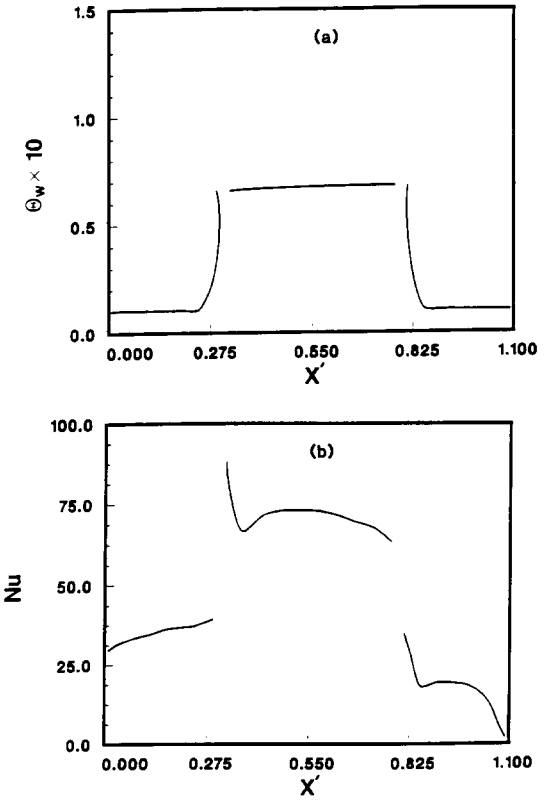

Figure 8 Configuration 7 (Table 2) with Re=6000 and the upstream face of the sensor at $x/H_c=1.5$: (a) surface temperature distribution of the sensor; (b) local Nusselt number distribution along the surface

simulation are not shown here; they are included, however, in Wietrzak.[13] Here, we present only a brief discussion. The surface temperature of the sensor was appreciably smaller than that for Re=6000, because a faster flow enhances cooling. The Nusselt number variation along the top face of the block was the weakest relative to all other cases examined in this study. The values of the Nusselt number, on the other hand, were the highest. Doubling the value of Re increased the maximum local heat transfer from the block to the fluid (minimum value of Nu) by approximately 15%.

Conclusions

This investigation was a numerical study of turbulent forced convective cooling of miniature electronic devices, such as the microbridge sensor. A two-equation k–ε model for turbulence was used to describe the flow. Among the results that stand out is the existence of a recirculation on top of the block simulating the sensor or chip. This recirculation is responsible for a "hump" (maximum) in the local Nusselt number variation along the top of the chip. In the absence of this recirculation, the Nusselt number decreases monotonically along the top of the chip.[3] The temperature of the heat generating top face of the block increased drastically when a layer of air was assumed to exist underneath the top surface. In reality, this layer of air is constructed by etching a pit in the silicon substrate under the heating elements of the top face. Increasing the height of the block strengthened all recirculations: before, after, and on top of the block. The temperature of the top surface was nearly constant in most cases in which uniform heat generation was assumed to exist throughout the length of this surface. When only a portion of the top surface of the block was assumed to generate heat, a local hot spot was observed. Finally, experimental studies are recommended to verify the present numerical findings.

Acknowledgment

Support for this work was provided by the Microswitch division of Honeywell Co. and by the National Science Foundation (grant no. ENG. 8451144) and is gratefully acknowledged. We thank E. Stern and R. Nickels of Microswitch for several illuminating discussions pertaining to the Microbridge sensor.

References

1 Harlow, H. H. and Welch, J. E. Numerical calculations of time-dependent viscous incompressible flow of fluid with free surface. *Physics of Fluids*, 1965, **8**(12), 2182–2189

2 Patankar, S. V. *Numerical Heat Transfer and Fluid Flow*. Hemisphere, New York, 1980

3 Davalath, J. and Bayazitoglu, Y. Forced convection cooling across rectangular blocks. *J. Heat Transfer*, 1987, **109**, 321–328

4 Zebib, A. and Wo, Y. K. A two dimensional conjugate heat transfer model for forced air cooling of an electronic device. International Packaging Conference, Orlando, FL, Oct. 22–24, 1985

5 Durst, F. and Rastogi, A. K. Theoretical and experimental investigations of turbulent flows with separation. *Turbulent Shear Flows I*, F. Durst, B. E. Launder, F. W. Schmidt, and J. H. Whitelaw (eds.). Springer-Verlag, New York, 1979, 208–219

6 Gosman, A. L., Khalil, E. E., and Whitelaw, J. H. The calculation of two-dimensional turbulent recirculating flows. *Turbulent Shear Flows I*, F. Durst, B. E. Launder, F. W. Schmidt, and J. H. Whitelaw (eds.). Springer-Verlag, New York, 1979, 237–255

7 Castro, J. P. Numerical difficulties in the calculation of complex turbulent flows. *Turbulent Shear Flows I*, F. Durst, B. E. Launder, F. W. Schmidt, and J. H. Whitelaw (eds.). Springer-Verlag, New York, 1979, 220–236

8 Chieng, C. C. and Launder, B. E. On the calculation of turbulent heat transfer downstream from an abrupt pipe expansion. *Num. Heat Transfer*, 1980, **3**, 189–207

9 Gooray, A. M., Watkins, C. B., and Aung, W. A two-pass procedure for the calculation of heat transfer in recirculating turbulent flow. *Num. Heat Transfer*, 1983, **6**, 423–440

10 Panton, R. L. *Incompressible Flow*. John Wiley & Sons, New York, 1984

11 Jones, W. P. and Launder, B. E. The prediction of laminarization with a two-equation model of turbulence. *Int. J. Heat and Mass Transfer*, 1972, **15**, 301–314

12 Jones, W. P. and Launder, B. E. The calculation of low-Reynolds-number phenomena with a two-equation model of turbulence. *Int. J. Heat Mass Transfer*, 1973, **16**, 1119–1130

13 Wietrzak, A. Numerical modelling of turbulent forced convective cooling of microelectronic devices. M.S. thesis, University of Illinois at Chicago, 1988

14 Doormaal, J. P. and Raithby, G. D. Enhancements of the SIMPLE method for predicting incompressible fluid flows. *Num. Heat Transfer*, 1984, **7**, 147–163

15 Emery, A. F. and Gessner, F. B. The numerical prediction of turbulent flow and heat transfer in the entrance region of a parallel plate duct. *J. Heat Transfer*, 1976, **98**, 594–600